19th Brazilian Congress of Thermal Sciences and Engineering
November 6th–10th, 2022, Bento Gonçalves - RS - Brazil

ENCIT2022-0136
SENSITIVITY ANALYSIS OF SMALL-SCALE VERTICAL-AXIS WIND TURBINES: IMPROVING THE DESIGN SPACE USING BÉZIER-GAN

Gabriel Bertacco dos Santos
Leandro Oliveira Salviano
São Paulo State University (UNESP), School of Engineering, Department of Mechanical Engineering
Avenida Brasil, 56. Ilha Solteira, São Paulo 15775-000, Brazil
gabriel.bertacco@unesp.br, leandro.salviano@unesp.br

Abstract. *Wind energy has emerged as an attractive alternative to the current fossil-fuel-based energy mix. The rapid growth of wind power plants around the world has inspired the development of novel technologies and more efficient equipment to meet the world's ever-growing energy needs. In this context, small-scale H-Darries vertical-axis wind turbines (VAWTs) are most appealing for harvesting wind energy in urban-like conditions. Nonetheless, the overall efficiency of H-Darries VAWTs still struggles with different complex aerodynamic phenomena. Seeking to improve the way optimization procedures for H-Darries VAWTs are currently done, we investigate the application of the BézierGAN parameterization in this context. For that, we adopt 3D computational fluid dynamics (CFD) simulations coupled with two sensitivity analysis methods. The results show that the BézierGAN solves the trade-off between shape variability and number of input parameters, providing high shape variability in a bounded, non-interactive, low-dimensional latent space. Therefore, we recommend this recently proposed parameterization method for future research and optimization of H-Darries VAWTs.*

Keywords: *renewable energy, vertical-axis wind turbine, generative neural network, airfoil parameterization, sensitivity analysis.*

1. INTRODUCTION

Despite efforts to improve the efficiency of energy consumption, demand for primary energy sources is presumed to rapidly increase in the near future, following populational and economic growth tendencies (Kc *et al.*, 2019). Currently, fossil fuels still count for the largest share in power generation around the world. However, the depletion of fossil fuel reserves, stricter environmental regulations, and global warming threats have urged the development of alternative sources for power generation. Among different renewable alternatives, wind-based power generation is considered the most cost-effective (Ghasemian *et al.*, 2017); additionally, it also presents the lowest relative greenhouse gas emission and the least water consumption (Evans *et al.*, 2009). For these reasons, the global cumulative installed wind energy capacity has been increasing substantially year after year, led specially by China, the United States, Europe, India, and Brazil.

While horizontal-axis wind turbines (HAWTs) continue to be commercially viable for large-scale energy generation, H-Darrieus vertical-axis wind turbines (VAWTs) combine interesting characteristics for small-scale power generation. As a whole, H-Darrieus VAWTs have recently received a growing interesting for power generation in the urban environment (Du *et al.*, 2019b; Kumar *et al.*, 2018) thanks to several distinct advantages, such as insensitivity to wind direction, ease maintenance, simple blade shapes, low cost, and low noise emission (Du *et al.*, 2019a). However, VAWTs are still reported to experience lower aerodynamic efficiency compared with modern HAWTs of equal scale (Du *et al.*, 2019b; Ghasemian *et al.*, 2017).

In part, the disparity in efficiency can be attributed to unsteady power conversion induced by large variations in the angle of attack perceived by the blades during each rotor revolution. Nevertheless, the unsteady nature of the power output is only a reflex of several complex flow phenomena taking place behind the blade motion—e.g., dynamic stall (Buchner *et al.*, 2018), blade–wake interference (Franchina *et al.*, 2019), and tip vortex shedding (Xu *et al.*, 2020). Therefore, the most significant challenge currently associated with employing small-scale H-Darrieus VAWTs for decentralized power generation concerns developing mechanisms capable of minimizing the aforementioned adverse aerodynamic effects.

To reduce these adverse aerodynamic effects and achieve better turbine performance, a few studies have proposed intrinsic auxiliary devices to either control the behavior of dynamic stall or the evolution of tip vortices; e.g., by employing

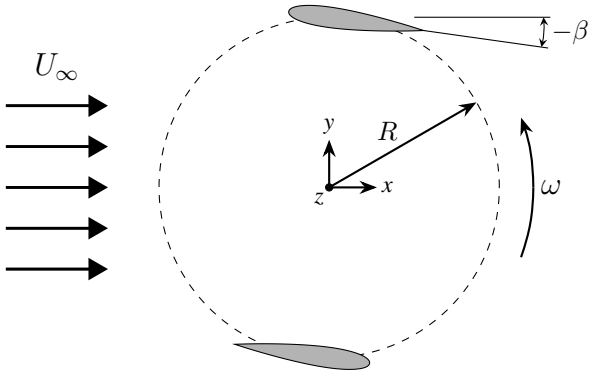

Figure 1. Schematic top view of a two-bladed H-Darrieus VAWT. R is the turbine radius; β is the blade pitch angle; U_∞ and ω are the freestream wind speed and the turbine angular speed, respectively.

active or passive pitch angle control (Abdalrahman *et al.*, 2017; Jain and Abhishek, 2016), or by adopting winglets (Zhang *et al.*, 2019; Xu *et al.*, 2020). Even though these methods improve the turbine performance, most studies continue to ignore the importance of the airfoil shape, which may equally influence the turbine aerodynamics. This aspect may be related to the lack of parameterization methods able to vary a wide range of shapes within a low-dimensional design space.

In this context, we investigate here the recently proposed Bézier-GAN parameterization, a deep generative adversarial network (GAN) that seeks to address most of the common pitfalls of other parameterization methods when coupled with optimization strategies. For that, we evaluate the turbine aerodynamics via 3D computational fluid dynamics (CFD) simulations. To evaluate the design space generated by the Bézier-GAN we then use two sensitivity analysis methods.

2. NUMERICAL SOLUTION

2.1 Physical and mathematical models

In this study we adopted a two-bladed H-Darrieus VAWT—see Fig. 1. The supporting arms were neglected in the context of this study. The blade chord lenght (c_b) is $0.225\,\mathrm{m}$, the blade height (h) is $1.02\,\mathrm{m}$, and the turbine radius (R) is $0.85\,\mathrm{m}$; thus, yielding a solidity (σ) of 0.397. Additionally, we considered that the turbine operate at a tip speed ratio (TSR) of 2.29 under a freestream wind speed of $7\,\mathrm{m/s}$.

For a proper characterization of the turbine aerodynamics, full-scale, time-dependent, 3D CFD simulations were adopted. As the Mach number for H-Darrieus VAWTs at urban-like wind conditions is lower than 0.2, the airflow can be considered incompressible (Balduzzi *et al.*, 2016). In this case, we face a classical problem of fluid dynamics in which the governing equations are described by the principle of conservation of mass and by the balance of momentum. Averaging these two equations on the longest time-scales of turbulence yields the Reynolds-averaged Navier–Stokes (RANS) equations, respectively, as follows:

$$\frac{\partial u_i}{\partial t} + \frac{\partial u_i}{\partial x_i} = 0 \tag{1}$$

and

$$\frac{\partial u_i}{\partial t} + u_i \frac{\partial u_i}{\partial x_j} = -\frac{1}{\rho}\frac{\partial p}{\partial x_i} - \frac{\partial}{\partial x_j}\left[\nu\left(\frac{\partial u_i}{\partial x_j} + \frac{\partial u_j}{\partial x_i} - \frac{2}{3}\delta_{ij}\frac{\partial u_i}{\partial x_i}\right)\right] + \frac{\partial}{\partial x_j}\left(-\overline{u_i' u_j'}\right), \tag{2}$$

where u and p are the flow velocity field and pressure field, respectively; ρ is the air density; ν is the air kinematic viscosity; and $\overline{u_i' u_j'}$ is the Reynolds stress tensor, which represents the rate of momentum transfer due to turbulent flow velocity fluctuations. To close the mathematical formulation, we model the Reynolds stress tensor via the shear stress transport (SST) turbulence formulation.

2.2 Numerical domain, boundary conditions, and solution strategy

The computational domain comprises two separated parts: a rotating core in which the turbine is located, and a fixed domain surrounding the core (Ma *et al.*, 2018; Rezaeiha *et al.*, 2017)—see Fig. 2. On the one hand, using a non-conformable interface between the rotating core and the fixed domain enables an ease approach to simulate the turbine rotation; on the other hand, special caution must be taken to ensure that the Courant–Friedrichs–Lewy (CFL) criterion is satisfied at the conservative sliding interface (Trivellato and Castelli, 2014).

In the governing equations we identify the flow velocity, pressure field, turbulence kinematic energy, and specific

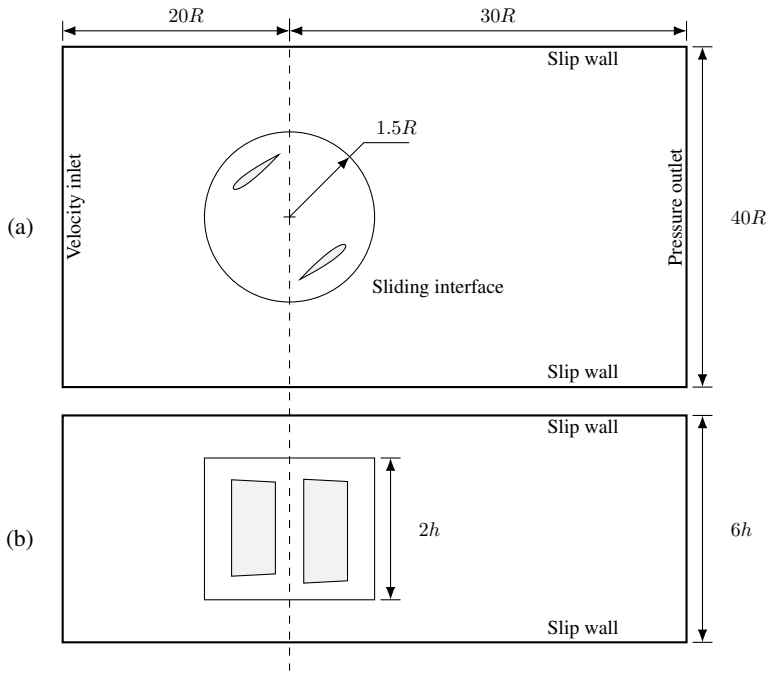

Figure 2. Schematic representation of the computational domain indicating dimensions and boundary conditions: (a) top view of the domain; (b) side view of the domain. R and h are the turbine radius and blade height, respectively.

turbulence dissipation rate as the unknowns—all four as functions of the spatial coordinates and the time. As we are to solve a set of partial differential equations, we must provide appropriate initial and boundary conditions. Here we adopted: (1) zero pressure gradient, prescribed uniform velocity, and $10\,\%$ turbulence intensity at the inlet; (2) zero gauge pressure and zero velocity gradient at the outlet; (3) impermeable, no-slip walls at the surface of the blades; (4) conservative flux at the sliding interface; and (5) impermeable, slip walls at the sides of the computational domain.

Lastly, to solve the governing equations under the abovementioned boundary conditions we chose the finite volume method (FVM) implemented in OpenFOAM (www.openfoam.com), the leading open-source software for CFD. Second order interpolation schemes were employed, and pressure–velocity coupling was done using the pressure-implicit split operators (PISO) algorithm (Issa *et al.*, 1986), as recommended by Lanzafame *et al.* (2014). Additionally, we adopted a time step corresponding to 360 steps per revolution. The convergence criterion for all variables in each time step was set to 1×10^{-5}.

2.3 Grid independence study

To quantify mesh discretization errors, a grid independence analysis was performed based on the grid convergence index (GCI) methodology (Celik *et al.*, 2008). For that, we adopted a baseline case consisting of a NACA 0015 blade with a pitch angle of -6°, similar to the one used by Li *et al.* (2016). For this baseline case we considered three mesh configurations with approximately 9.7×10^6 (coarse), 18×10^6 (medium), and 29.7×10^6 (fine) cells in the rotating core, yielding a refinement ratio of approximately 1.3. The number of cells in the stationary domain was kept constant, with approximately 1.6×10^6 cells. The mesh characteristics on the blades were also kept constant, i.e., number of layers, expansion ratio, and total thickness.

Table 1 shows that using the medium-sized mesh results in a numerical uncertainty of less than $0.5\,\%$. In a sense, even the coarse-sized mesh could be adopted, which would result in a numerical uncertainty of $4\,\%$. However, depending on the airfoil shape, with this few elements the mesh generator could struggle to properly represent the blade surface. Thus, we decided to use the medium-sized mesh, even though it increases the processing time per simulation.

2.4 Validation

We compared the results of the numerical model with the experimental data provided by Li *et al.* (2016), considering the same geometric and operational conditions (Table 2). Figure 3 shows that our numerical model agrees with the experimental data. The experimental data and the numerical model present an azimuthally averaged torque coefficient (C_q) of 8.19×10^{-2} and 7.75×10^{-2}, respectively; thus, yielding a mean relative difference of $5.3\,\%$.

Table 1. Data for the GCI analysis. The number of cells represents the cell count in the rotating core, and $\overline{C_p}$ represents the azimuthally averaged power coefficient. The refinement ratio was taken with respect to the coarse mesh. GCI_{21} reports the numerical uncertainty of the medium mesh with respect to the fine mesh.

	Coarse (3)	Medium (2)	Fine (1)
Number of cells	9,702,615	17,964,448	29,740,350
Refinement ratio	–	1.3	1.69
$\overline{C_p}$	0.345	0.355	0.354

$GCI_{21} = 0.277\,\%$

Table 2. Characteristics of the validation model, mimicking the geometric and operational conditions of the experimental study presented in (Li *et al.*, 2016).

Parameters	Description
Airfoil profile	NACA 0015
Blade chord lenght (c_b)	$0.225\,\mathrm{m}$
Pitch angle (β)	-6°
Blade height (h)	$1.02\,\mathrm{m}$
Turbine radius (R)	$0.85\,\mathrm{m}$
Freestream velocity (U_∞)	$7\,\mathrm{m/s}$
Tip speed ratio	2.29

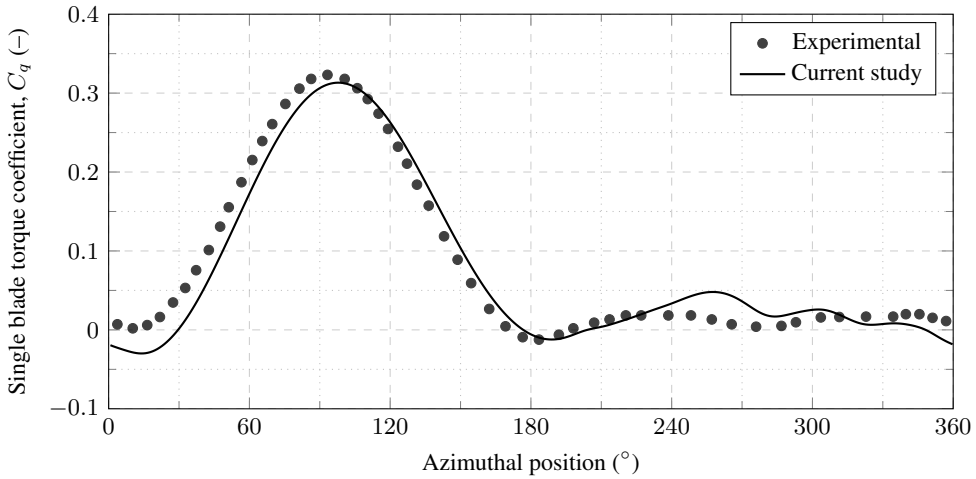

Figure 3. Comparison between the experimental (Li *et al.*, 2016) and the numerical profiles of instantaneous torque coefficient (C_q) for a single blade. Refer to Table 2 for a description of the geometric and operational conditions.

3. AIRFOIL PARAMETERIZATION

3.1 Background

Airfoil parameterization methods are responsible for mapping a set of input parameters onto a smooth surface representation (e.g., the NACA families, PARSEC, and FFD). These methods serve two main purposes: they guarantee geometric reproducibility and easy integration into optimization strategies. However, even though the most common airfoil parameterization methods were meant to be integrated with optimization strategies, there are at least two main issues associated with these methods. 1) In most cases one has to constrain the bounds of the input parameters so that the parameterization does not excessively generate invalid shapes. 2) There is a trade-off between shape variability and the number of input parameters: i.e., few input parameters may not be able to adequately explore the space of possible designs (e.g., four-digit NACA series), whereas many input parameters may incur in the well-known curse of dimensionality (e.g., PARSEC).

To some extent dimensionality reduction methods can be adopted to address point #2—e.g., principal component analysis (PCA) and singular value decomposition (SVD). However, these methods do not seek to minimize the generation

of invalid aerodynamic shapes. In an attempt to address both issues, Chen and Fuge (2021) have recently proposed the Bézier-GAN, a deep GAN that seeks to reduce the design space dimensionality and, at the same time, minimize mapping to a domain of invalid aerodynamic shapes.

3.2 Bézier-GAN as a smooth shape synthetizer

Typical GANs consist of two main blocks: a generator G and a discriminator D. The generator takes in random latent variables z (noise) and generates some synthesized data $G(z)$. The discriminator takes in a data sample x and predicts the probability $D(x)$ of the sample being real or fake. This is an adversarial game: the generator tries to approximate the generative distribution P_z to the real-world data distribution P_{data}; the discriminator tries not be fooled by the generator. This game can be mathematically expressed as

$$\min_G \max_D V(G,D) = \mathbb{E}_{x\sim P_{\text{data}}}[\log D(x)] + \mathbb{E}_{z\sim P_z}[\log(1 - D(G(z))] \tag{3}$$

Most GANs do not implement methods to regularize the latent variables, making almost impossible to directly translate input variations into interpretable design modifications. This single aspect can hinder the design space exploration and, consequently, the optimization procedure. To overcome this issue, the InfoGAN (Chen *et al.*, 2016) adopts the concept of mutual information maximization between latent variables and synthesized samples as a way to produce interpretable, disentangled latent spaces.

Even though the InfoGAN meets most of the necessary requirements for a promising airfoil parameterization method for aerodynamic optimization, it does not guarantee orthogonal latent variables. Additionally, the InfoGAN can produce nonsmooth and/or discontinuous shapes quite often. To compensate this last aspect, the Bézier-GAN modifies the InfoGAN generator such that it only generates shapes that conform to Bézier curves (Chen and Fuge, 2021), assuring smoothness and continuity for any synthesized sample. Note that the latent and noise variables are automatically normalized in the range $[0, 1]$; thus, there is no need for choosing appropriate bounds for each variable. For more details on the Bézier-GAN implementation we direct interested readers to Chen *et al.* (2020) and Chen and Fuge (2021).

3.3 Dataset preparation and network training

As the Bézier-GAN depends on data for training on, we must define a dataset of valid aerodynamic shapes. For that, we use the UIUC airfoil database[1], which provides more than 1600 real-world airfoil shapes for various applications, ranging from low Reynolds number airfoils for model aircraft to jet transports and wind turbines. The UIUC database consist of individual files representing the discrete 2D coordinates of each airfoil design. A B-spline interpolation was used to generate a consistent representation of the original database designs.

The Bézier-GAN training followed the same process described in Chen *et al.* (2020). For the current work, we adopted a four-dimensional latent space ($l = 4$) and a null noise space ($z = 0$) as a way to compare with other low-dimensional parameterization methods, like the four-digit NACA series. The resulting network is able to characterize a wide range of airfoil shapes with four interpretable, disentangled latent variables. Figure 4 compares samples from the training dataset with synthesized samples from the resulting Bézier-GAN. Note that the synthesized samples easily outperform the four-digit NACA series in design variability, representing a larger design space with the same number of input variables.

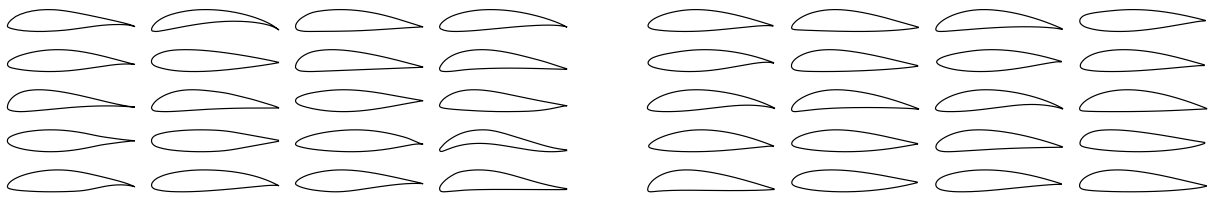

(a) (b)

Figure 4. Examples of airfoil shapes. (a) Samples from the UIUC database. (b) Samples of synthesized airfoils via the Bézier-GAN (latent dimension = 4 and noise dimension = 0).

4. SENSITIVITY ANALYSIS

Sensitivity analysis methods have been widely adopted as adjunctive tools in several investigations. These methods explore the relationship between model output and input parameters, providing qualitative and/or quantitative information regarding the effects of the different input parameters and their variance on the model output (Ge *et al.*, 2015).

[1] https://m-selig.ae.illinois.edu/ads.html

4.1 The elementary effects (EEs) method

Considering the numerical approach proposed previously, we choose to adopt the EEs method (Morris, 1991), which introduces a qualitative sensitivity analysis method for high-dimensional and/or computationally expensive models. The EEs method is based on individually randomized one-at-a-time perturbation of the input parameters—or also called factors. For each input factor, the method computes the overall influence (μ) and higher order effects (σ) on the model output; thereby, determining which factors influence the model output the most.

For a model with k independent factors, each model input X_i is assumed to vary p times, yielding a k-dimensional p-level region of experimentation (Campolongo *et al.*, 2007). Considering a given value of $\mathbf{X}$, the EE of the i^{th} input parameter can be defined as

$$d_i(\mathbf{X}) = \left[\frac{y(\mathbf{X}+\boldsymbol{\Delta}_i) - y(\mathbf{X})}{(\mathbf{X}+\boldsymbol{\Delta}_i) - \mathbf{X}}\right], \tag{4}$$

where $\boldsymbol{\Delta}$ is the step vector. Morris (1991) suggests sampling r elementary effects for each input variable via an efficient design that constructs r trajectories of $(k+1)$ points in the input space, each providing k elementary effects—one per factor. Thus, the total cost of the experiment becomes $r(k+1)$. With r trajectories it is then possible to compute μ and σ as

$$\mu_i = \frac{1}{r}\sum_{j=1}^{r}\left|d(\mathbf{X})_i^j\right| \tag{5}$$

and

$$\sigma_i^2 = \frac{1}{r-1}\sum_{j=1}^{r}\left[d(\mathbf{X})_i^j - \mu_i\right]^2. \tag{6}$$

4.2 The smoothing spline ANOVA (SS-ANOVA) method

As a quantitative method for sensitivity analysis we chose the SS-ANOVA, a variance-based model that is able to compute both main and two-way interactions for each input parameter (Salviano *et al.*, 2021). We can express a two-way ANOVA decomposition as

$$f(\mathbf{X}) = f_0 + \sum_{j=1}^{p} f_j(X_j) + \sum_{j<i}^{p} f_{j,i}(X_j, X_i). \tag{7}$$

The SS-ANOVA decomposition can be built as a minimization problem for the least squares functional L that estimates the model f fitness while subject to a constraint J that controls the model smoothness and avoids overfitting. The contribution π of each input factor k can be then represented as

$$\pi_k = \frac{f_k^{\mathrm{T}}\sum_{j=1}^{p} f_j}{\left(\sqrt{\sum_{j=1}^{p} f_j \sum_{j=1}^{p} f_j}\right)^2} \tag{8}$$

where f_k^{T} is a column vector representing the decomposition of individual variables and $\sum_{j=1}^{p} f_j$ is the sum of the decomposition of all sampling points.

4.3 Sampling strategy

For the SS-ANOVA there are no restrictions to how a design of experiment (DoE) should be generated. On the other hand, as a one-at-a-time method, the EE requires the evaluation points to be sampled in a specific way, i.e., each two points in a same trajectory r_i should differ in only one coordinate X_j. Thus, in the current work we adopted the radial sampling proposed by Campolongo *et al.* (2011). To assemble the DoE using the radial sampling one must define a baseline vector $\mathbf{b}$ and an auxiliary vector $\mathbf{q}$. See Table 3 for an example.

We sampled the baseline vector via uniform latin hypercube sampling (ULHS) and the auxiliary vector via the Sobol's quasi-random sequence. The Sobol's sequence tend to repeat the values 0.25, 0.5, and 0.75 in the first few rows. Therefore, to achieve different step/coordinate values for each trajectory in the final DoE we discarded the first four rows of the Sobol's sequence, as suggested by Campolongo *et al.* (2011). Finally, we generated ten trajectories ($r = 10$) using the

Table 3. Example of a single trajectory generated via the radial design proposed by Campolongo *et al.* (2011). b_i and q_i are the baseline and the auxiliary points, respectively.

Point	Coordinate
1	$\{b_0, b_1, b_2, \ldots, b_k\}$
2	$\{q_0, b_1, b_2, \ldots, b_k\}$
3	$\{b_0, q_1, b_2, \ldots, b_k\}$
4	$\{b_0, b_1, q_2, \ldots, b_k\}$
$\vdots$	$\vdots$
$k+1$	$\{b_0, b_1, b_2, \ldots, q_k\}$

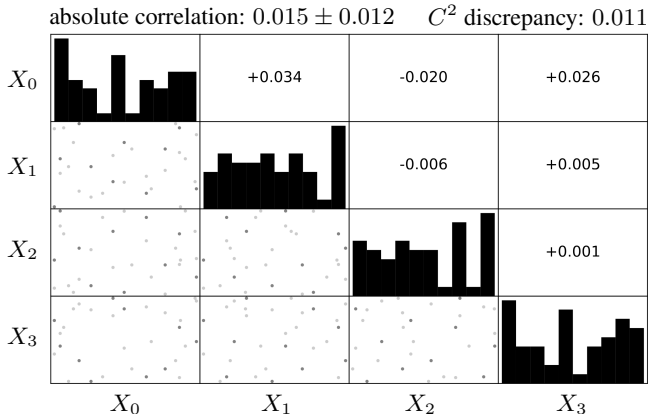

Figure 5. Scatter matrix for the generated DoE showing the dispersion of the parameters in the experimentation region and the correlation for each two parameters.

radial sampling, resulting in a total of 50 points. Figure 5 shows the dispersion of the parameters in the experimentation region.

5. RESULTS AND DISCUSSIONS

Figure 6 shows an approximation of the probability density function (PDF) of the azimuthally averaged power coefficient ($\overline{C_p}$) as a metric for the dispersion of the aerodynamic efficiency within the generated DoE. Note that by varying only the airfoil shape the aerodynamic efficiency of the H-Darrieus VAWT varies greatly. Additionally, values of interest—i.e., $\overline{C_p} \geq 0.2$—represent only a small fraction of the design space. This single aspect highlights the importance of the airfoil profile in the context of H-Darrieus VAWTs. Therefore, a naïve choice may strongly hinder the turbine aerodynamic efficiency.

Regarding the sensitivity analysis, Fig. 7 presents the sensitivity measures computed via the EEs method. Following the terminology defined by Vanrolleghem *et al.* (2015), we note that all four factors do not present strong interaction

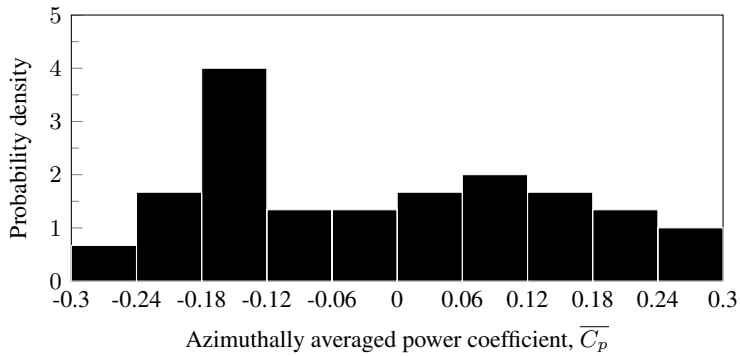

Figure 6. Approximation of the probability density function of the azimuthally averaged power coefficient ($\overline{C_p}$) within the generated DoE.

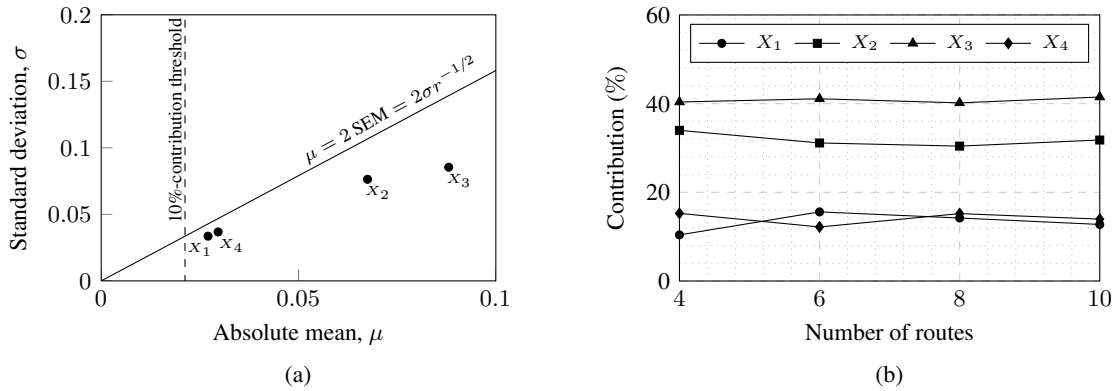

Figure 7. Sensitivity measures by the EEs method. (a) Analysis of factor importance and interactions for ten routes ($r = 10$). (b) Analysis of the influence of the number of routes on the individual contributions of each factor as a convergence metric.

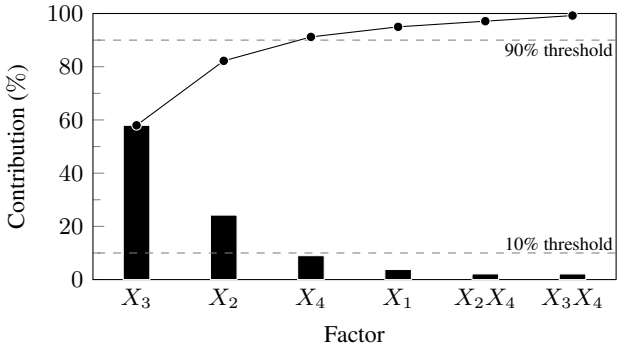

Figure 8. Sensitivity measures via the SS-ANOVA method. Bar plots represent the individual contributions of the main effects and the principal interaction effects. The scatter plot represents the cumulative contribution.

effects, as they lay below the line $\mu = 2\,\mathrm{SEM}$, where SEM represents the standard error of the mean, computed as $\mathrm{SEM} = 2\,\sigma r^{-\frac{1}{2}}$. Also, all four factors should be considered important, as they lay above the $10\,\%$-contribution threshold. Additionally, the latent variables X_2 and X_3 have the strongest influence on the turbine aerodynamics, accounting for approximately $75\,\%$ of the total influence.

Looking to the results of the SS-ANOVA (Fig. 8), even though the degree of importance of each factor slightly differs from the EEs method, we note that the factor ranking is consistent in both methods. Differently from the EEs method, the SS-ANOVA classifies the latent variables X_1 and X_4 below the $10\,\%$-contribution threshold. Additionally, the two strongest interaction effects—i.e., X_2X_4 and X_3X_4—present only negligible influence, with lower importance than all four main effects. Thus, further confirming the results of the EEs method. Just for comparison, four-digit NACA shapes present strong two-way interactions in the context of H-Darrieus VAWTs (Barros, 2021).

Although not a requirement, the absence of interacting effects constitute an important aspect for optimization problems. Optimization problems that present significant interaction effects can be much harder to reach the global minimum either via direct optimization or via metamodel strategies. Additionally, strong interacting effects may directly impact the choice of the optimization algorithm—e.g., gradient-based methods may not perform well in such cases because of their dependence of the initial conditions, which in turn may increase the total cost of the experiment.

One interesting aspect of the absence of interacting effects comes from the parameterization method itself. As highlighted in Section 3, the Bézier-GAN is built upon the classical InfoGAN, which aims to maximize the mutual information between the latent variables and the synthesized shapes. By doing so, the network learns not only human-interpretable representations but also the very heart of the data distribution, meaning that the network can understand the principal components of shape variability in a dataset of real-world airfoils that underwent various improvement processes. Nonetheless, further research should be done on this topic to confirm whether the Bézier-GAN would always produce latent spaces with negligible interaction effects.

Lastly, as the latent space lacks interactions between the factor, it can be interpreted in the light of individual contributions. Hence, noninfluential variables may be fixed at their nominal values during the optimization procedure, further reducing the total cost of the experiment. Even though the two analysis methods do not strictly agree on the individual contributions, they incontestably highlight the predominance of the latent variables X_2 and X_3.

6. CONCLUSIONS

In the current study we investigated the applicability of the recently proposed Bézier-GAN parameterization in the context of H-Darrieus VAWTs as a way to improve the design space for optimization procedures. Compared to traditional parameterization methods, the Bézier-GAN compiles some of the most appealing aspects for an optimization. It solves the well-known trade-off between shape variability and number of parameters, providing high shape variability in a bounded, low-dimensional latent space.

Additionally, a sensitivity analysis via both the EEs method and the SS-ANOVA highlighted that the latent space does not present significant interacting factors. Even though the aerodynamic response greatly varies as a consequence of a design space with shape variability, the search for optimum profiles may strongly benefit from the absence of interactions. Therefore, we recommend the Bézier-GAN parameterization method for future research and optimization of H-Darrieus VAWTs.

7. ACKNOWLEDGEMENTS

This research was supported by resources supplied by the Center for Scientific Computing (NCC/GridUNESP) of the São Paulo State University (UNESP).

8. REFERENCES

Abdalrahman, G., Melek, W. and Lien, F.S., 2017. "Pitch angle control for a small-scale Darrieus vertical axis wind turbine with straight blades (H-Type VAWT)". *Renewable Energy*, Vol. 114, pp. 1353–1362. doi:10.1016/j.renene.2017.07.068.

Balduzzi, F., Bianchini, A., Maleci, R., Ferrara, G. and Ferrari, L., 2016. "Critical issues in the CFD simulation of Darrieus wind turbines". *Renewable Energy*, Vol. 85, pp. 419–435. doi:10.1016/j.renene.2015.06.048.

Barros, P.H.M., 2021. *Análise de sensibilidade do desempenho aerodinâmico de uma turbina eólica vertical Darrieus de pequena escala*. Master's thesis, São Paulo State University (UNESP), Ilha Solteira, Brazil.

Buchner, A.J., Soria, J., Honnery, D. and Smits, A.J., 2018. "Dynamic stall in vertical axis wind turbines: Scaling and topological considerations". *Journal of Fluid Mechanics*, Vol. 841, pp. 746–766. doi:10.1017/jfm.2018.112.

Campolongo, F., Cariboni, J. and Saltelli, A., 2007. "An effective screening design for sensitivity analysis of large models". *Environmental Modelling & Software*, Vol. 22, No. 10, pp. 1509–1518. doi:10.1016/j.envsoft.2006.10.004.

Campolongo, F., Saltelli, A. and Cariboni, J., 2011. "From screening to quantitative sensitivity analysis. A unified approach". *Computer Physics Communications*, Vol. 182, No. 4, pp. 978–988. doi:10.1016/j.cpc.2010.12.039.

Celik, I.B., Ghia, U., Roache, P.J., Freitas, C.J., Coleman, H. and Raad, P.E., 2008. "Procedure for Estimation and Reporting of Uncertainty Due to Discretization in CFD Applications". *Journal of Fluids Engineering*, Vol. 130, No. 7, p. 078001. doi:10.1115/1.2960953.

Chen, W., Chiu, K. and Fuge, M.D., 2020. "Airfoil Design Parameterization and Optimization Using Bézier Generative Adversarial Networks". *AIAA Journal*, Vol. 58, No. 11, pp. 4723–4735. doi:10.2514/1.J059317.

Chen, W. and Fuge, M., 2021. "BezierGAN: Automatic Generation of Smooth Curves from Interpretable Low-Dimensional Parameters". *arXiv:1808.08871*.

Chen, X., Duan, Y., Houthooft, R., Schulman, J., Sutskever, I. and Abbeel, P., 2016. "InfoGAN: Interpretable Representation Learning by Information Maximizing Generative Adversarial Nets". *arXiv:1606.03657*.

Du, L., Ingram, G. and Dominy, R.G., 2019a. "Experimental study of the effects of turbine solidity, blade profile, pitch angle, surface roughness, and aspect ratio on the H-Darrieus wind turbine self-starting and overall performance". *Energy Science & Engineering*, Vol. 7, No. 6, pp. 2421–2436. doi:10.1002/ese3.430.

Du, L., Ingram, G. and Dominy, R.G., 2019b. "A review of H-Darrieus wind turbine aerodynamic research". *Proceedings of the Institution of Mechanical Engineers, Part C: Journal of Mechanical Engineering Science*, Vol. 233, No. 23-24, pp. 7590–7616. doi:10.1177/0954406219885962.

Evans, A., Strezov, V. and Evans, T.J., 2009. "Assessment of sustainability indicators for renewable energy technologies". *Renewable and Sustainable Energy Reviews*, Vol. 13, No. 5, pp. 1082–1088. doi:10.1016/j.rser.2008.03.008.

Franchina, N., Persico, G. and Savini, M., 2019. "2D-3D Computations of a Vertical Axis Wind Turbine Flow Field: Modeling Issues and Physical Interpretations". *Renewable Energy*, Vol. 136, pp. 1170–1189. doi:10.1016/j.renene.2018.09.086.

Ge, Q., Ciuffo, B. and Menendez, M., 2015. "Combining screening and metamodel-based methods: An efficient sequential approach for the sensitivity analysis of model outputs". *Reliability Engineering & System Safety*, Vol. 134, pp. 334–344. doi:10.1016/j.ress.2014.08.009.

Ghasemian, M., Ashrafi, Z.N. and Sedaghat, A., 2017. "A review on computational fluid dynamic simulation techniques for Darrieus vertical axis wind turbines". *Energy Conversion and Management*, Vol. 149, pp. 87–100. doi:10.1016/j.enconman.2017.07.016.

Issa, R., Gosman, A. and Watkins, A., 1986. "The computation of compressible and incompressible recirculating flows by a non-iterative implicit scheme". *Journal of Computational Physics*, Vol. 62, No. 1, pp. 66–82. doi:10.1016/0021-9991(86)90100-2.

Jain, P. and Abhishek, A., 2016. "Performance prediction and fundamental understanding of small scale vertical axis wind turbine with variable amplitude blade pitching". *Renewable Energy*, Vol. 97, pp. 97–113. doi:10.1016/j.renene.2016.05.056.

Kc, A., Whale, J. and Urmee, T., 2019. "Urban wind conditions and small wind turbines in the built environment: A review". *Renewable Energy*, Vol. 131, pp. 268–283. doi:10.1016/j.renene.2018.07.050.

Kumar, R., Raahemifar, K. and Fung, A.S., 2018. "A critical review of vertical axis wind turbines for urban applications". *Renewable and Sustainable Energy Reviews*, Vol. 89, pp. 281–291. doi:10.1016/j.rser.2018.03.033.

Lanzafame, R., Mauro, S. and Messina, M., 2014. "2D CFD Modeling of H-Darrieus Wind Turbines Using a Transition Turbulence Model". *Energy Procedia*, Vol. 45, pp. 131–140. doi:10.1016/j.egypro.2014.01.015.

Li, Q., Maeda, T., Kamada, Y., Murata, J., Kawabata, T., Shimizu, K., Ogasawara, T., Nakai, A. and Kasuya, T., 2016. "Wind tunnel and numerical study of a straight-bladed Vertical Axis Wind Turbine in three-dimensional analysis (Part II: For predicting flow field and performance)". *Energy*, Vol. 104, pp. 295–307. doi:10.1016/j.energy.2016.03.129.

Ma, N., Lei, H., Han, Z., Zhou, D., Bao, Y., Zhang, K., Zhou, L. and Chen, C., 2018. "Airfoil optimization to improve power performance of a high-solidity vertical axis wind turbine at a moderate tip speed ratio". *Energy*, Vol. 150, pp. 236–252. doi:10.1016/j.energy.2018.02.115.

Morris, M.D., 1991. "Factorial Sampling Plans for Preliminary Computational Experiments". *Technometrics*, Vol. 33, No. 2, pp. 161–174. doi:10.1080/00401706.1991.10484804.

Rezaeiha, A., Kalkman, I. and Blocken, B., 2017. "CFD simulation of a vertical axis wind turbine operating at a moderate tip speed ratio: Guidelines for minimum domain size and azimuthal increment". *Renewable Energy*, Vol. 107, pp. 373–385. doi:10.1016/j.renene.2017.02.006.

Salviano, L.O., Gasparin, E.E., Mattos, V.C.N., Barbizan, B., Saltara, F., de Mello, P.E.B., Dezan, D.J. and Yanagihara, J.I., 2021. "Sensitivity analysis and optimization of a CO2 centrifugal compressor impeller with a vaneless diffuser". *Structural and Multidisciplinary Optimization*, Vol. 64, No. 3, pp. 1607–1627. doi:10.1007/s00158-021-02914-2.

Trivellato, F. and Castelli, M.R., 2014. "On the Courant–Friedrichs–Lewy criterion of rotating grids in 2D vertical-axis wind turbine analysis". *Renewable Energy*, Vol. 62, pp. 53–62. doi:10.1016/j.renene.2013.06.022.

Vanrolleghem, P.A., Mannina, G., Cosenza, A. and Neumann, M.B., 2015. "Global sensitivity analysis for urban water quality modelling: Terminology, convergence and comparison of different methods". *Journal of Hydrology*, Vol. 522, pp. 339–352. doi:10.1016/j.jhydrol.2014.12.056.

Xu, W., Li, G., Wang, F. and Li, Y., 2020. "High-resolution numerical investigation into the effects of winglet on the aerodynamic performance for a three-dimensional vertical axis wind turbine". *Energy Conversion and Management*, Vol. 205, p. 112333. doi:10.1016/j.enconman.2019.112333.

Zhang, T., Elsakka, M., Huang, W., Wang, Z., Ingham, D.B., Ma, L. and Pourkashanian, M., 2019. "Winglet design for vertical axis wind turbines based on a design of experiment and CFD approach". *Energy Conversion and Management*, Vol. 195, pp. 712–726. doi:10.1016/j.enconman.2019.05.055.

9. RESPONSIBILITY NOTICE

The authors are solely responsible for the printed material included in this paper.